Low Temperature Electrical Properties of CVD Graphene on LiNbO₃: Acoustic Studies

© *I.L. Drichko* [1], *I.Yu. Smirnov* [1,¶], *Yu.M. Galperin* [1,2], *P.A. Dementev* [1], *M.G. Rybin* [3]

[1] Ioffe Institute,
194021 St. Petersburg, Russia
[2] Department of Physics, University of Oslo,
P. O. Box 1048 Blindern, 0316 Oslo, Norway
[3] Prokhorov Institute of General Physics of the Russian Academy of Sciences,
119991 Moscow, Russia

¶ E-mail: ivan.smirnov@mail.ioffe.ru

Contactless acoustic methods were used to determine electrical parameters — electrical conductivity, carrier mobility and their concentration — in single-layer graphene deposited on the surface of lithium niobate.

1. Introduction

Graphene is the unique two-dimensional material of XXI century. Its main advantage is unprecedented carriers mobility, caused by presence of free electron on *p*-orbital, that is delocalized along the whole graphene monolayer and can move with high velocity as massless fermion. Due to this particular unique property of graphene the bright future was predicted for its application in nano-electronics. However, in actual practice it turned out that it is very hard to reach the record-high values of carriers mobility in graphene, let alone the manufacturing of samples, that can be reproduced on an industrial scale. Graphene quality and possibility of its application in nanoelectronics are usually characterized with charge carriers mobility in this material. Thus, the task of quality control by means of analysis of charge carriers mobility in graphene is of great relevance. The highest values of charge carriers mobility, up to $10^6 \, \text{cm}^2/\text{V} \cdot \text{s}$, were achieved in freely suspended quasineutral graphene, produced by the method of epitaxial growth on silicon carbide in vacuum at low temperatures [1]. However, this method of graphene producing is poorly scaled and expensive. For mass commercial synthesis of graphene the method of chemical vapor deposition (CVD) of graphene on copper foil surface is used. This method is easier to implement and more cost effective than the epitaxial growth. Charges mobility in graphene pro-duced by CVD method is lower, but also can be high under certain conditions, reaching the values of up to $3.5 \cdot 10^5 \, \text{cm}^2/\text{V} \cdot \text{s}$ [2].

For material optimizations it is very important to have the reliable procedure of mobility measurement. The most popular approach for charges mobility measurement is the production of a field transistor with graphene channel [3].

This method allows to make measurements with high accuracy, but preparation to measurements requires more efforts, particularly lithography and etching of graphene, as well as metal contacts deposition on graphene. Another method (4-contact, as per Van der Pauw in magnetic field [4]) is an alternative option of mobility measurement. However, the probes contacting with sample can result in sample damage.

The third method of mobility measurement is a terahertz spectroscopy [5]. This is a non-contact method, allowing to define the charges mobility in graphene. The method allows to study the distribution of conductivity and mobility over the sample surface. But sensitivity of the method is relatively low ($\sigma < 0.1 \, \text{mS}$).

In this study we use non-contact method of charges mobility measurement in graphene at low temperatures using analysis of distribution of surface acoustic waves (SAW) along the interface of piezodielectric (LiNbO₃) and graphene. Simultaneous measurement of velocity and attenuation of SAW allows to define the complex conductance of graphene on SAW frequency (see, for instance, review [6]).

In this study the results of measurement of two graphene samples, produced using the method of chemical vapor deposition on copper foil surface, and passed to piezodielec-tric LiNbO₃ are demonstrated. Using the abovementioned technique [6] the electrophysical properties of graphene were studied and its charge carriers mobility was calcu-lated. Graphene samples, different in surface morphology, that is caused by peculiarities of graphene synthesis and possibility to control the process with high accuracy, were used in the study. Samples are different in copper foil temperature during synthesis, particularly, differences in temperature by $10-20°C$ between the samples result in variation of grains quantity in polycrystal sample of

graphene and, as a result, various charges scattering on their boundaries. The procedure of measurements is described in the study in detail, and differences in electrophysical parameters of samples with various surface morphology are described.

2. Samples and experimental procedure

In this study we examined two graphene samples, produced using the method of chemical vapor deposition on copper foil surface from gas mixture of argon, hydrogen and methane at temperature of $850°C$ and reduced pressure of $100\,\mathrm{mbar}$. The main differential characteristic of graphene synthesis method is a method of copper foil heating with direct passage of current through it. This method allows to control the heating and cooling rate with high accuracy, while the temperature is measured by pyrometer through inspection window in vacuum chamber. Detailed information in synthesis method is presented in studies [7,8]. Disadvantages of this method include small temperature gradient of copper foil of $10-20°C$ at a distance of $10\,\mathrm{mm}$ (in sample with dimensions of $20 \times 20\,\mathrm{mm}$ the temperature varies from $850°C$ in the center of the sample to $830°C$ at sample edges). During study we used one synthesized sample with dimensions of $20 \times 20\,\mathrm{mm}$, divided into several parts with dimensions of $7 \times 10\,\mathrm{mm}$, two of which were passed to piezoelectric (lithium niobate). In this study the sample 1 had the reduced temperature of $830°C$ during synthesis, while sample 2 had the temperature of $850°C$ during synthesis. Both graphene samples were passed from copper foil to lithium niobate surface using the standard method of „wet" transition with polymethylmethacrylate as a supporting polymer and ammonium persulphate as an etchant for copper.

Piezoelectric properties and high quality of $LiNbO_3$ crystals give significant advantages for studying the two-dimensional and quasi-two-dimensional materials. Particularly, strong piezoelectric effect of $LiNbO_3$ allows to use oscillating electrical fields, generated by surface acoustic wave (SAW) at its propagation over the piezocrystal and entering the low-dimensional system, placed on its surface [9]. As a result, the absorption, Γ, and velocity, v, of SAW depend on the electrical characteristics of the surface layer and can be used for quantitative determination of the latter. This is the main idea behind the acoustic method of low-dimensional materials analysis, that we used for various systems (see for review, e.g., [6]).

Three essential advantages make this technique rather prospective.

(1) The method does not require electrical contacts, therefore the results do no depend on them.

(2) Electronic contributions to absorption and SAW velocity depend on magnetic field, and these dependencies allow to separate the electronic contributions from lattice contributions.
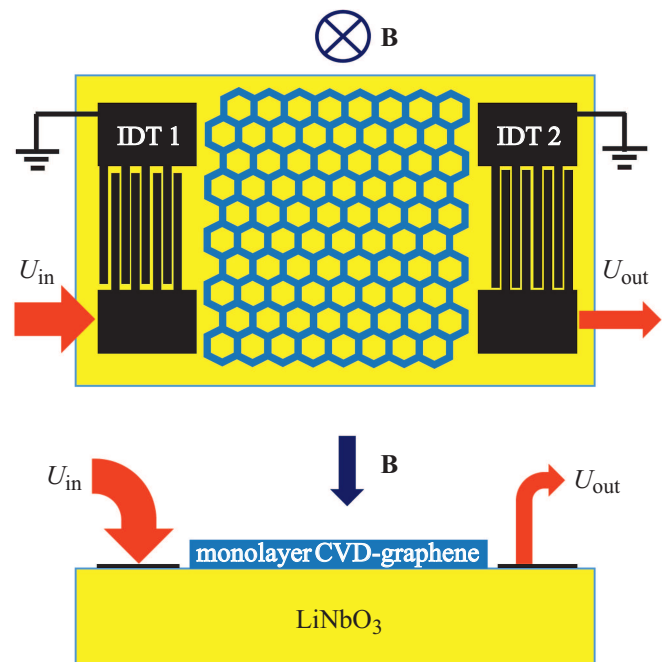

Figure 1. Scheme of acoustic experiment. U_{in} and U_{out} are the input and output signals, **B** is the magnetic field.

(3) Relation of dynamic high-frequency (HF) conductivity, absorption and sound velocity includes values, measured experimentally.

For this experiment the monolayer graphene film was deposited on polished surface of lithium niobate, on which the converters IDT 1 and IDT 2 (of gold) were preformed for generation and receiving the surface acoustic waves. Figure 1 demonstrates the experimental scheme. SAW frequencies were 28, 85, 140, 197 and 252 MHz (odd harmonics of the main converter frequency of 28 MHz). Holder with sample was put to cryostat with superconducting magnet and cooled to temperatures of $1.7-4.2\,\mathrm{K}$. Absorption and variation of SAW velocity of various frequencies depending on magnetic field of up to 8 T were measured during the experiment.

Absorption and variation of SAW velocity propagation are defined by a sum of two contributions caused by crystal lattice and charge carriers. Since the lattice contributions in non-magnetic materials do not depend on magnetic field, for separation of these contributions it is naturally to use the dependencies of acoustic characteristics on magnetic field.

In approximation, linear to SAW amplitude, the contributions of charge carriers are defined with complex dynamic conductance, $\sigma(\omega, \mathbf{k}) \equiv \sigma_1(\omega, \mathbf{k}) - i\sigma_2(\omega, \mathbf{k})$, that generally depends on frequency of SAW ω, and its wave vector $\mathbf{k}$. Relation between SAW propagation characteristics and conductance is the following (see, for instance, [6]):

$$\Gamma = k \cdot (K^2/2) \cdot (\sigma_1/\sigma_\mathrm{M})/[(1 + \sigma_2/\sigma_\mathrm{M})^2 + (\sigma_1/\sigma_\mathrm{M})^2)], \quad (1)$$

$$\Delta v/v = (K^2/2)\big((1 + \sigma_2/\sigma_\mathrm{M})/\big[(1 + \sigma_2/\sigma_\mathrm{M})^2 + (\sigma_1/\sigma_\mathrm{M})^2\big].$$

Here, $k \equiv |\mathbf{k}|$, $K^2/2 = 2.25 \cdot 10^{-2}$ — electromechanical constant of lithium niobate, $\sigma_{1,2}$ — real and imaginary parts of dynamic conductivity $\sigma(\omega)$ per square (conductance); $\sigma_M = v_0 \cdot (\varepsilon_1 + \varepsilon_{gr})$, v_0 — SAW velocity at $B = 0$; ε_1, ε_{gr} — dielectric constants of lithium niobate and graphene, respectively. During calculations we used values $\varepsilon_1 = 50$, $\varepsilon_{gr} = 6.9$ [10].

From the simultaneously measured absorption and variation of SAW velocity the complex conductance of graphene can be calculated, $\sigma(\omega) = \sigma_1(\omega) - i\sigma_2(\omega)$. From analysis of these values it can be concluded that σ_1 and σ_2 weakly depend on frequency over the whole examined frequency range, while $\sigma_2(\omega) \ll \sigma_1(\omega)$. Such relation supports the metal nature of graphene layer conductivity, while the dynamic conductance $\sigma_1(\omega)$ is close to static conductance $\sigma(B) \equiv \sigma_{xx}(\omega = 0, B)$.

It should be noted that in the examined system the graphene layer is a polycrystal line material with significant electrons scattering over grain boundaries. This is indicated by, particularly, measured conductivity value. We suppose that such material is not characterized with Dirac cones anymore, but can be rather characterized as a system of conductivity electrons with concentration n and quadratic spectrum at effective mass m^* and momentum relaxation time τ.

In non-quantizing magnetic field the conductivity of such surface layer is defined as per formula

$$\sigma(B) = \sigma_0/[1 + (\omega_c \tau)^2], \qquad (2)$$

where σ_0 is the conductivity in the absence of magnetic field, ω_c is the cyclotron frequency. When using Drude equation for electrons with isotropic quadratic spectrum, $\omega_c = eB/m^*c$, where c is the light velocity. In strong magnetic field, when the following condition is met

$$(\omega_c \tau)^2 = (\mu B/c)^2 \gg 1, \qquad (3)$$

where μ is the charge carriers mobility, $\sigma(B) \sim B^{-2}$. If we build the dependence of the experimentally defined conductivity on $1/B^2$, and it is linear, from this linear dependence we can define the slope A and relation

$$\mu^2/c^2 = \sigma_0/A. \qquad (4)$$

If we take a point on the experimental curve $\sigma(B)$, where the strong field condition (3) is not met, after simple calculations we get

$$\sigma(0) = \sigma(B)/[1 - \sigma(B) \cdot B^2/A]. \qquad (5)$$

Thus, determination of electronic characteristics using acoustic method is as follows:

1) building of the experimental dependence $\sigma(1/B^2)$ in the area of strong magnetic fields, calculation of the slope A of linear dependence $\sigma = A/B^2$;

2) determination of $\sigma(0)$ as per formula (5);

3) determination of mobility as per formula (4) and current concentration as per formula

$$n = \sigma(0)/e\mu. \qquad (6)$$

This method of graphene characteristics determination is rather approximate, since we know only the approximate graphene film length (~ 7 mm). Besides, limited reproducibility of the results of various experiments on the same sample also impacts the accuracy.

3. Experimental results

In the study we examined 2 samples, with monolayer CVD graphene, deposited on lithium niobate surface using the same method, described above. However, the samples characteristics are significantly different. Measurements of absorption Γ and $\Delta v/v$ were made in temperature interval of $(1.7-4.2)$ K, in frequency range of $(28-300)$ MHz in magnetic fields of up to 8 T. Temperature variation of Γ and $\Delta v/v$ in zero magnetic field was studied for sample 2 at frequencies of 30 and 140 MHz.

3.1. SAW absorption at $B = 0$

In sample 1 the large absorption of SAW, ~ 30 dB/cm, that grows with temperature decrease, is observed even at room temperature.

In sample 2 the absorption coefficient Γ is ~ 15 dB/cm at room temperature and also increases with temperature decrease. Figure 2 shows the dependencies of absorption and variation of SAW velocity in the absence of magnetic field in sample 2.

Figure 3 shows the dependencies of $\Delta\Gamma = \Gamma(4.2\,\text{K}) - \Gamma(300\,\text{K})$ and $\Delta v/v$ on B for sample 1.

As shown in the figure, the value of SAW electronic absorption for sample 1 in magnetic field of 8 T is very small and does not exceed value of 1.2 dB/cm, while SAW velocity almost does not depend on B. Values of Γ and $\Delta v/v$ for sample 2 are significantly bigger than for sample 1.

For electrical characteristics determination we use the procedure of experimental results processing, described above.

Sample 1

Figure 4, a shows the dependence of experimentally defined σ_1 on $1/B^2$. In the area of magnetic field of $8-5$ T this dependence is linear with slope $d\sigma/d(1/B^2) = 4 \cdot 10^{18}$ (σ — in CGS units, while B — in G).

For sample 1 the following characteristics were observed using formulas (4)$-$(6): $\sigma(B = 0) = 0.013$ Ohm^{-1}, $\mu = 5.4 \cdot 10^3$ cm^2/V·s, $n = 1.5 \cdot 10^{13}$ cm^{-2}.

Figure 4, b shows the dependences of experimentally defined conductivity on magnetic field (black) and calculated as per formula (2) (red) with values presented above. It is shown that the red curve describes the experiment well.
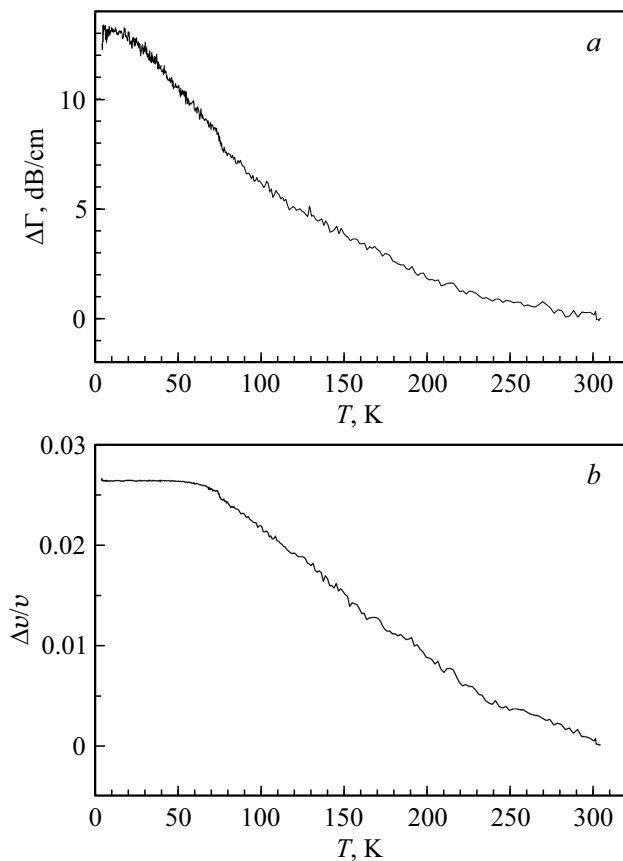
Figure 2. Dependence (*a*) of absorption coefficient $\Delta\Gamma$ and (*b*) $\Delta v/v$ on temperature T; $f = 30\,\mathrm{MHz}$, $B = 0\,\mathrm{T}$.

Sample 2

Figure 5, *a* shows the experimental dependence of σ_1 on $1/B^2$. In the area of magnetic field of $8-2\,\mathrm{T}$ the dependence is linear with slope in $d\sigma/d(1/B^2) = 4.9 \cdot 10^{17}$ (σ — in CGS units, while B — in G). For sample 2 the following characteristics ($1.7\,\mathrm{K}$, $85\,\mathrm{MHz}$) were observed using the formulas (4)−(6):

$$\sigma(B = 0) = 0.043\,\mathrm{Ohm}^{-1},$$

$$\mu = 2.8 \cdot 10^4\,\mathrm{cm}^2/\mathrm{V} \cdot \mathrm{s},$$

$$n = 1 \cdot 10^{13}\,\mathrm{cm}^{-2}.$$

Figure 5, *b* shows the experimental dependence of conductivity on magnetic field (black) and calculated (red) as per formula (2) with values defined using the method, presented above. It is shown that the red curve with these parameters describes the experiment well.

Figure 6 illustrates experimental dependences of conductivity σ_1 on magnetic field B at various temperatures, measured at frequency $f = 140\,\mathrm{MHz}$ (*a*), and dependence of σ_1 on B for various SAW frequencies at $T = 1.7\,\mathrm{K}$ (*b*).

The figures show that conductivity weakly depends on T and f, while the average values for temperature dependence in magnetic field of $7\,\mathrm{T}$ are equal to $\sigma_1 = (4.0 \pm 0.3) \cdot 10^{-5}\,\mathrm{Ohm}^{-1}$, while for frequency dependence $\sigma_1 = (7.6 \pm 1.0) \cdot 10^{-5}\,\mathrm{Ohm}^{-1}$ within measurement error. However, it can be seen that the average values differ almost by factor 2. The reason is that measure-


Figure 3. *a* is the dependence of Γ and $\Delta v/v$ on magnetic field B; $f = 140\,\mathrm{MHz}$, $T = 1.7\,\mathrm{K}$; sample 1. *b* is the dependence of Γ and $\Delta v/v$ on magnetic field B; $f = 85\,\mathrm{MHz}$, $T = 1.7\,\mathrm{K}$; sample 2.
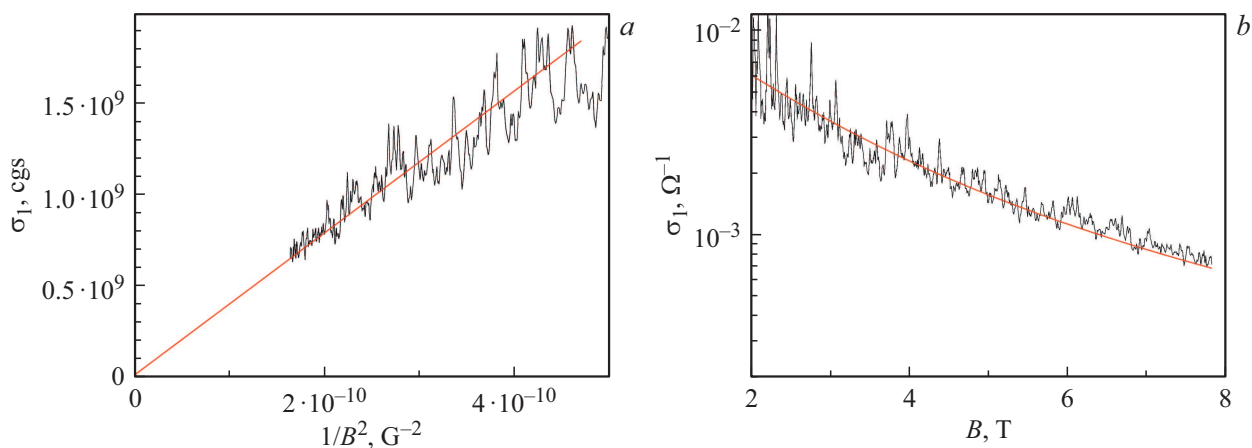
Figure 4. *a* is the dependence of σ_1 (CGS) on $1/B^2$ (G^{-2}); *b* is the dependence of σ_1 (Ohm^{-1}) on B (T) for sample 1, $f = 140$ MHz, $T = 1.7$ K.
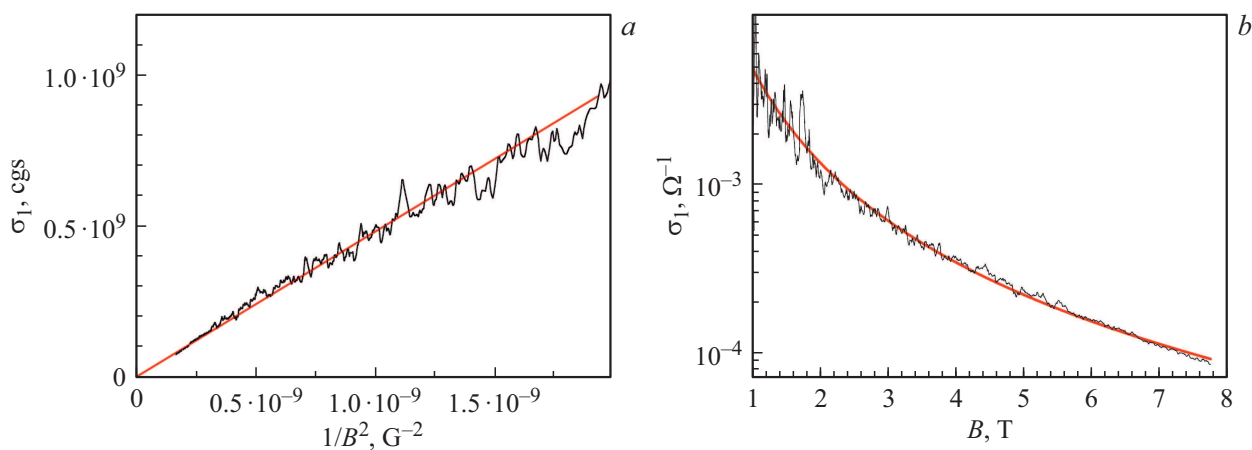
Figure 5. *a* is the dependence of σ_1 (CGS) on $1/B^2$ (G^{-2}); *b* is the dependence of σ_1 (Ohm^{-1}) on B (T) for sample 2, $f = 85$ MHz, $T = 1.7$ K.
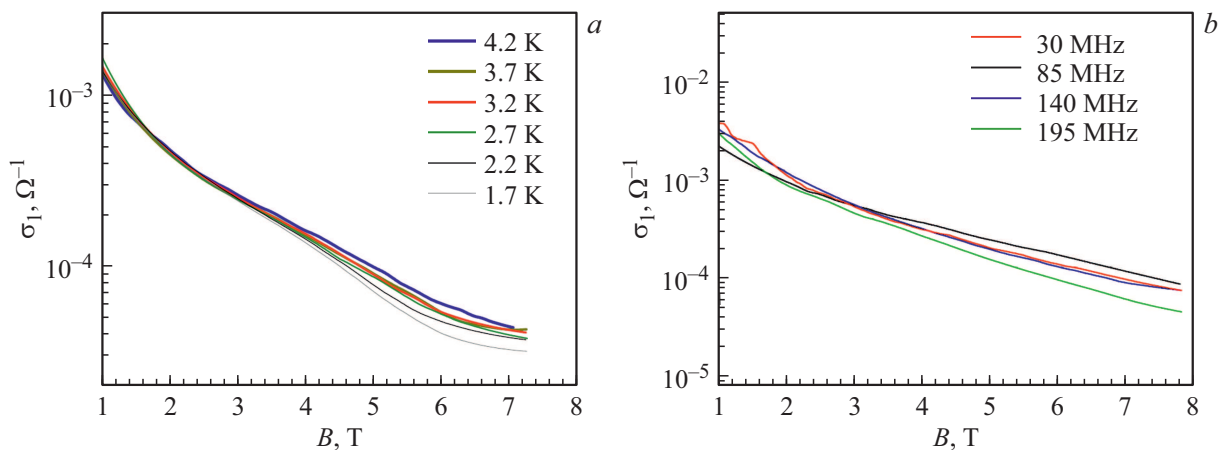
Figure 6. *a* is the dependence of σ_1 on magnetic field B at various temperatures, $f = 140$ MHz; *b* is the dependence of σ_1 on B for various frequencies of SAW at $T = 1.7$ K. (Colored version of the figure is presented in electronic version of the article).
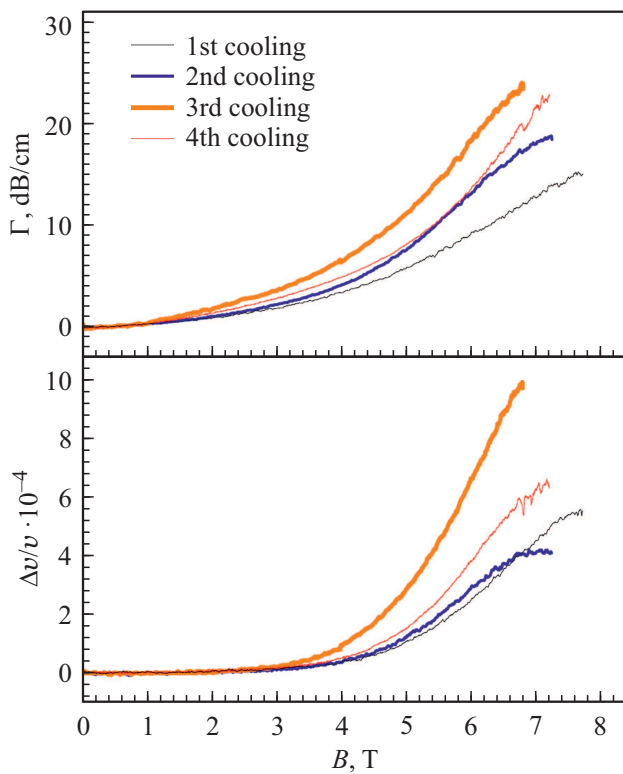
Figure 7. Dependence of Γ and $\Delta v/v$ on magnetic field B; $f = 140\,\mathrm{MHz}$, $T = 1.7\,\mathrm{K}$ at various cooling cycles.

ments of temperature dependence were made in a single day (within single cooling cycle), while the frequency dependences — in different days (within different cooling cycles).

We observed that with each new cooling cycle for graphene sample, deposited on lithium niobate, the dependences of values of absorption and variation of sound velocity on magnetic field were not reproduced. This is shown in Fig. 7 for $f = 140\,\mathrm{MHz}$ and $T = 1.7\,\mathrm{K}$.

Calculation using formulas $(3)-(5)$ showed that conductivity $\sigma(0)$, defined from these curves, is within a range from $4 \cdot 10^{-3}$ to $1.3 \cdot 10^{-2}\,\mathrm{Ohm}^{-1}$, mobility μ is within a range from $9.4 \cdot 10^{3}$ to $1.8 \cdot 10^{4}\,\mathrm{cm}^2/\mathrm{V} \cdot \mathrm{s}$, while concentration n is from $2 \cdot 10^{12}$ to $4.5 \cdot 10^{12}\,\mathrm{cm}^{-2}$.

3.2. Atomic force microscopy (AFM)

Samples were studied using methods of atomic force and kelvin-probe microscopy. The main attention was drawn to areas of relatively large $(30 \times 30\,\mu\mathrm{m})$ size. Typical images for samples 1 and 2 are presented in Fig. 8.

It is well seen that sample 1 is covered with a large amount of linear defects, which probably represent graphene wrinkles, appeared after sample cooling and heating cycles. Such peculiarities are also seen on sample 2, but in significantly less amount. The specified difference of the samples is more noticeable in potential distribution images (Fig. 9).

Two types of defects are shown on sample 1. Extended peculiarities, combined into the common network, probably correspond to grain boundaries of polycrystal graphene. Also, the round peculiarities are observed, that we associate with islands of the second graphene layer. It should be noted that the majority of linear objects, observed on topography image, is not reflected in surface potential distribution.

Potential distribution on sample 2 is much more homogeneous. Several areas with reduced potential, that we also
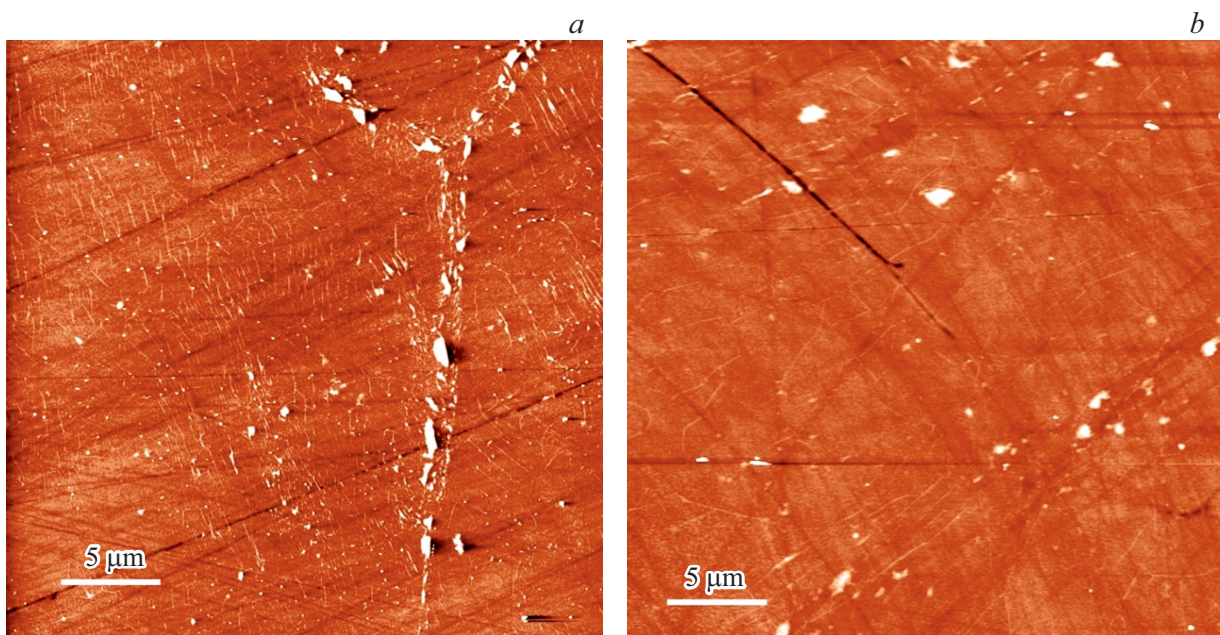

Figure 8. Topography of areas of $30 \times 30\,\mu\mathrm{m}$ for sample 1 (a) and sample 2 (b).

a

b
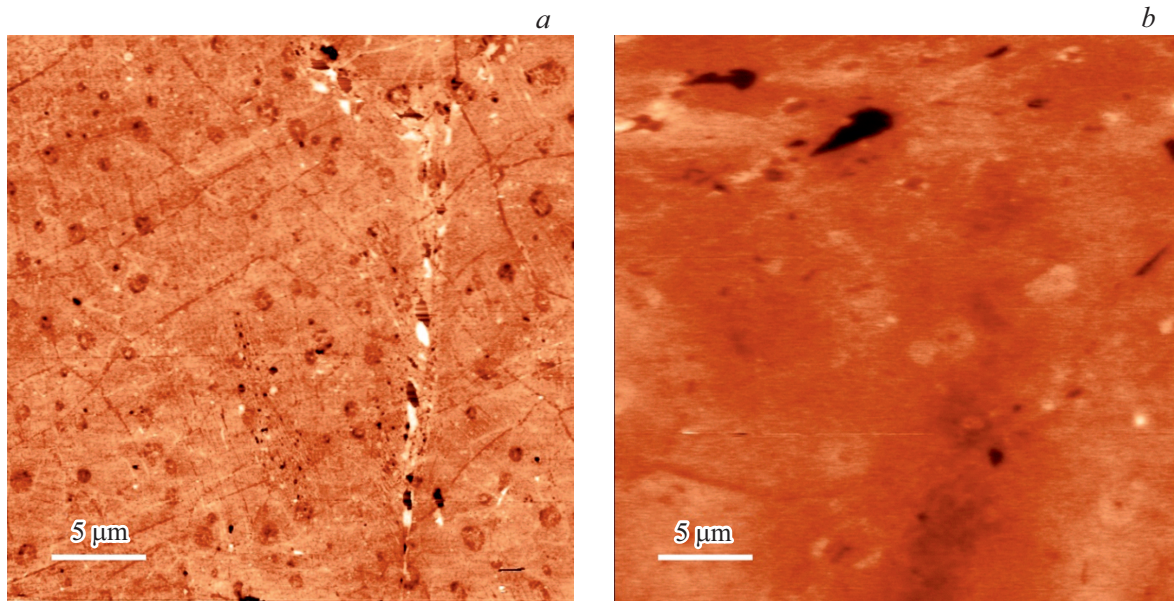
Figure 9. Distribution of surface potential of areas of $30 \times 30\,\mu$m for sample 1 (*a*) and sample 2 (*b*). The darker color shades correspond to lower values of surface potential.

associate with the islands of the second graphene layer, are observed. Drop-like defect, observed in the upper part, corresponds to rupture in graphene layer.

4. Discussion of results

Let's start the results discussion with dependence of SAW absorption coefficient Γ on temperature at $B = 0$. In study [8] it was specified that for monolayer undoped graphene, deposited on SiO₂/Si, resistance at room temperature in the absence of magnetic field was about $300-1000$ Ohm per square. With such resistance the SAW absorption with charge carriers is very low, $\Gamma < 1$ dB/cm, therefore the high SAW absorption, observed in the experiment, and its weak dependence on temperature probably indicate the absorption (scattering) of SAW with structure defects in polycrystal film of graphene. Absorption in sample 1 was much higher than in sample 2, that is presumably caused by the fact that sample 1 has much more defects than sample 2. This is confirmed with the results of samples study using the methods of atomic force and kelvin-probe microscopy at room temperature.

As per Figs. 8 and 9, the individual graphene grains as part of polycrystal line film are well-visualized on sample 1. Also, the wrinkles are observed on surface due to sequential processes of sample cooling and heating. Despite the same polycrystal line nature of sample 2, no grain boundaries are observed on it.

We suppose that increase of absorption (scattering) of SAW during sample cooling is related to increase of amount of defects, for instance, ruptures in film, that are „cured" during sample heating after measurements. Increase

of defects concentration during samples cooling happens randomly, as per Fig. 7.

Dependence of σ_1 on magnetic field, temperature and frequency indicates the metal nature of conductivity at low temperature, while in sample 1 with higher amount of defects the carriers mobility is less than in sample 2. Relation $\sigma_1 > \sigma_2$ also indicates the metal nature of conductivity.

It turned out that values of charge carriers mobility in graphene (5400 and 28000 cm²/V · s), obtained using non-contact acoustic method, are much higher than mobility values ($1100-1500$ cm²/V · s), obtained by the measurement of the volt-ampere characteristics (VAC) of graphene field transistor (GFT), made of similar samples [11,12]. It seems, it can be explained with several factors. Firstly, the measurements of volt-ampere characteristics in GFT were made at room temperature. Secondly, preparation for these measurements assumes multiple lithography and polymer application, as well as other process manipulations with samples, that result in their degradation. Thirdly, when measuring the VAC in GFT, graphene contacts with metal, that can significantly change the electronic structure of graphene and make contributions to its charge carriers mobility.

5. Conclusion

Non-contact acoustic methods use for studying the low-temperature electrical properties of monolayer CVD graphene, deposited on lithium niobate surface, allowed to define its new characteristics. These characteristics include variation (increase) of amount of defects at samples cooling from room temperature to 4.2 K and random nature of these defects formation at various cooling cycles. The

latter property expressed in limited reproducibility of the measured absorption and variation of SAW velocity. Along with determination of the material electrical characteristics, the mechanism of low-temperature conductivity was defined.

Funding

Conflict of interest

The authors declare that they have no conflict of interest.

References

[1] M. Orlita, C. Faugeras, R. Grill, A. Wysmolek, W. Strupinski, C. Berger, W.A. de Heer, G. Martinez, M. Potemski. Phys. Rev. Lett., **107**, 216603 (2011).

[2] L. Banszerus, M. Schmitz, S. Engels, J. Dauber, M. Oellers, F. Haupt, K. Watanabe, Takashi Taniguchi, Bern Beschoten, C. Stampfer. Sci. Adv., **1**, e1500222 (2015).

[3] Nianduan Lu, Lingfei Wang, Ling Li, Ming Liu. Chinese Phys. B, **26**, 036804 (2017).

[4] Rui-Song Ma, Qing Huan, Liang-Mei Wu, Jia-Hao Yan, Yu-Yang Zhang, Li-Hong Bao, Yun-Qi Liu, Shi-Xuan Du, Hong-Jun Gao. Chinese Phys. B, **26**, 066801 (2017).

[5] J.D. Buron, F. Pizzocchero, P.U. Jepsen, D.H. Petersen, J.M. Caridad, B.S. Jessen, T.J. Booth, P. Boggild. Sci. Rep., **5**, 12305 (2015).

[6] I.L. Drichko, I.Yu. Smirnov, A.V. Suslov, Y.M. Galperin, L.N. Pfeiffer, K.W. West. Low Temperature Phys., **43**, 86 (2017); doi: 10.1063/1.4975107

[7] M. Rybin, A. Pereyaslavtsev, T. Vasilieva, V. Myasnikov, I. Sokolov, A. Pavlova, E. Obraztsova, A. Khomich, V. Ralchenko, E. Obraztsova. Carbon, **96**, 196 (2016).

[8] M.G. Rybin, V.R. Islamova, E.A. Obraztsova, E.D. Obraztsova. Appl. Phys. Lett., **112**, 033107 (2018).

[9] A. Wixforth, J.P. Kotthaus, G. Weinmann. Phys. Rev. Lett., **56**, 2104 (1986).

[10] J. Fang, W.G. Vandenberghe, M.V. Fischetti. Phys. Rev. B, **94**, 045318 (2016).

[11] Y. Matyushkin, S. Danilov, M. Moskotin, V. Belosevich, N. Kaurova, M. Rybin, E.D. Obraztsova, G. Fedorov, I. Gorbenko, V. Kachorovskii, S. Ganichev. Nano Lett., **20**, 7296 (2020).

[12] A. Gayduchenko, G.E. Fedorov, M.V. Moskotin, D.I. Yagodkin, S.V. Seliverstov, G.N. Goltsman, A.Yu. Kuntsevich, M.G. Rybin, E.D. Obraztsova, V.G. Leiman, M.S. Shur, T. Otsuji, V.I. Ryzhii. Nanotechnology, **29**, 245204 (2018).